RSC Advances

PAPER

View Article Online
View Journal | View Issue

Cite this: *RSC Adv.*, 2017, **7**, 4710

Catalytic performance of gallium oxide based-catalysts for the propane dehydrogenation reaction: effects of support and loading amount

Chun-Tao Shao, Wan-Zhong Lang,* Xi Yan and Ya-Jun Guo*

The different materials (ZSM-5, SBA-15, γ-Al_2O_3 and SiO_2) were used as supports for Ga_2O_3-based catalysts for the propane dehydrogenation reaction, and the effect of Ga_2O_3 content (1–9 wt%) for xGa_2O_3/SBA-15 catalysts on the catalytic activity was discussed. It is found that the supports determine the porous features, the state and dispersion of Ga species, and the acid–base properties of the corresponding catalysts. The existence of strong acid sites in catalyst can lead to more well-dispersed Ga species. The satisfied catalytic performances are obtained over $5Ga_2O_3$/ZSM-5 and $5Ga_2O_3$/SBA-15 catalysts. Among the Ga_2O_3-based catalysts with different supports, the $5Ga_2O_3$/ZSM-5 sample exhibits the highest catalytic activity, which possesses the maximum well-dispersed gallium species and high dehydrogenation efficiency gallium ions ($Ga^{\delta+}$ cations, $\delta < 2$), and the $5Ga_2O_3$/SBA-15 catalyst exhibits the highest catalytic stability. Furthermore, as for the xGa_2O_3/SBA-15 samples, the $5Ga_2O_3$/SBA-15 sample exhibits the best catalytic performance. The initial propane conversion and propylene selectivity are above 32.0% and 90.0% respectively, and a final propane conversion of 17.0% is obtained after 30 h reaction. With the increase of Ga loading, the Ga species are easily agglomerated and destroy the structural integrity of the SBA-15 support, which is unfavorable to the propane dehydrogenation reaction.

Received 23rd November 2016
Accepted 27th December 2016

DOI: 10.1039/c6ra27204e

www.rsc.org/advances

1 Introduction

Propylene is a major raw chemical for the petrochemical industry. In recent years, more attention has been paid to the catalytic dehydrogenation of propane to propylene because the growing demand for propylene is beyond the production capacity of conventional hydrocarbon steam cracking and catalytic cracking processes.[1–3] The catalytic dehydrogenation of propane is an endothermic process, which needs a relatively high reaction temperature to obtain a high propylene yield. Nevertheless, under such high temperatures, the undesirable side reactions such as hydrogenolysis, cracking and coke deposition are inevitable.[4,5]

Currently, many studies are devoted to developing novel and potential catalysts in propane dehydrogenation (PDH), such as ceria-based catalysts,[6] calcined hydrotalcite-supported platinum catalysts,[7] Sn/SiO_2 catalysts,[8] Pd-based catalysts,[9] mesoporous carbons, gallium oxide-based catalysts[10,11] and so on. Among these, gallium oxide-based catalysts have been recognized as new promising alkane dehydrogenation materials due to their unique capability to activate hydrocarbon species and excellent catalytic efficiency as compared to conventional Cr_2O_3- and V_2O_5-based catalysts.[12–16] For instance, Nakagawa *et al.*[14] proposed that the commercial Ga_2O_3 had exceptionally high activity for the dehydrogenation of ethane to ethylene, and they found that β-Ga_2O_3 exhibited the highest dehydrogenation activity among all of the polymorphs due to its abundant surface acid sites.

The support effects of catalysts were also considered to be an important topic. Previous studies[11,16–19] reported that the Ga_2O_3 species were dispersed on different supports including TiO_2, MgO, Al_2O_3, ZrO_2, ZSM-5, HZSM-48 and MWW zeolites for alkane dehydrogenation reaction. Many literatures verified that acidity of support evidently influenced the catalytic performance of the supported catalysts. For example, Shen *et al.*[20] reported that the stability and selectivity of Ga_2O_3/HZSM-5 catalyst in the propane dehydrogenation were enhanced by increasing the Si/Al ratio of HZSM-5 support. XU *et al.*[16] reported that Ga_2O_3/TiO_2, Ga_2O_3/Al_2O_3 and Ga_2O_3/ZrO_2 showed better activity for the dehydrogenation of propane to propylene than Ga_2O_3/SiO_2 and Ga_2O_3/MgO due to the more acid sites in medium to strong strength. Wang *et al.*[19] revealed that Ga/ITQ-2 exhibited higher selectivity and better stability in propane dehydrogenation reaction as compared with those of Ga/MCM-22, due to the higher surface area and relatively less strong acid sites.

Since gallium oxide-based catalysts were found to have good alkane dehydrogenation properties,[14,15,21] several investigations

The Education Ministry Key Laboratory of Resource Chemistry and Shanghai Key Laboratory of Rare Earth Functional Materials, Department of Chemistry and Chemical Engineering, Shanghai Normal University, 100 Guilin Road, Shanghai 200234, China. E-mail: wzlang@shnu.edu.cn; guoyajun@shnu.edu.cn; Fax: +86-21-64321951; Tel: +86-21-64321951

attempted to elucidate the reasons of high catalytic performance. The previous studies reported that the gallium oxides (Ga_2O_3, GaO^+) were the most species presented on the catalyst after calcination and were readily reduced during pretreatment with hydrogen.[16,22–24] The various gallium species (Ga_2O_3, GaO^+ and Ga^+) as active constituents exhibited different performances for light alkane dehydrogenation reaction.[25] In addition, Nowak *et al.*[26] also reported the dispersion of Ga_2O_3 species varied with different supports. However, the effects of supports on the state of gallium species have not been fully understood, especially the causes of these changes.

Among these support materials, alumina is extensively used as catalyst support due to its surface acidic properties and desirable textual properties. Nevertheless, the stability of catalyst is still not very satisfactory.[27,28] As regards ZSM-5 zeolite, it has some particular physical properties such as unique three-dimensional channels, relatively large surface area and adjustable Si/Al ratio. Especially it can hinder the formation of large hydrocarbon molecules due to the unique framework and channel structure, which are beneficial to the catalytic stability. Therefore, ZSM-5 is widely used in propane dehydrogenation reaction.[29,30] Besides, as advanced mesoporous materials, SBA-15 and nano-silica are often employed as supports for catalysts. Generally, SBA-15 is characterized by its ordered porous structure, high specific surface area and high thermal stability, and the certain pore volume of mesoporous materials and the free of acid sites can greatly resist the formation of coke.[31,32] Nano-silica also has the characteristics of large surface area, chemical stability and cheapness.[33] It is obvious that the catalysts using different supports may show the distinctive catalytic properties. Hence it is necessary to discuss the influences of the different supports on the catalytic performances for Ga_2O_3-based catalysts in propane dehydrogenation. Nevertheless, according to what I'm informed, the detailed investigations of different supports on the catalytic performances for Ga_2O_3-based catalysts are rarely reported, especially with SBA-15 material as support.

The objective of this work is to study the influences of different supports on the state of gallium and the catalytic performances of Ga_2O_3-based catalysts for propane dehydrogenation, and further discuss the optimum Ga_2O_3 loading content and reaction parameters of Ga_2O_3/SBA-15 catalysts in propane dehydrogenation. A series of different supports (ZSM-5, SBA-15, γ-Al_2O_3 and SiO_2) were prepared, and then loaded with Ga_2O_3 species by impregnation method. The as-prepared samples were characterized by several state-of-art characterizations. The structure–activity relationships of the catalysts were analyzed and elucidated.

2 Experimental

2.1 Catalyst preparation

The mesoporous SBA-15 was prepared according to the previous literature.[4] The triblock copolymer P123 (EO20PO70EO20, M_n = 5800, from Aldrich) was used as the structure-directing agent, and tetraethyl orthosilicate (TEOS) was used as the silica source. In brief, 4 g of P123 was added in 160 mL of 2 mol L^{-1} HCl aqueous solution and stirred for 0.5 h until fully dissolved, and then 6.4 g of tetraethyl orthosilicate (TEOS) was slowly dripped to the prepared mixture solution with strong stirring at 40 °C for 24 h to get white gel. The resulting gel was subsequently transferred into a Teflon autoclave and held at 100 °C for 24 h. The obtained sample was filtered and washed using deionized water, and dried in a desiccator overnight. Then, the sample was calcined in air at 550 °C for 4 h to remove the structure-directing agent to obtain final SBA-15 powder. Then, the synthesized SBA-15 together with other three commercial materials including γ-Al_2O_3 (S_{BET}: 180 m^2 g^{-1}, 80–100 mesh), ZSM-5 (Si/Al = 45–80) and SiO_2 (particle size = 50 nm) were used as supports. The supported Ga_2O_3 catalysts were prepared by impregnating the different supports with an aqueous solution of $Ga(NO_3)_3 \cdot xH_2O$ (Aldrich). Afterward, the prepared samples were aged at room temperature for 4 h, and then the catalysts were dried overnight in air at 100 °C, followed by calcination at 550 °C for 4 h in air. The $5Ga_2O_3$/X and xGa_2O_3/SBA-15 catalysts were got. Unless otherwise specified, as for the $5Ga_2O_3$/X catalysts, the loading of Ga_2O_3 was 5 wt%, where X represents the different support. The prefix x of xGa_2O_3/SBA-15 samples indicates the different amounts of Ga_2O_3 content varying from 1 to 9 wt%.

2.2 Catalyst characterizations

2.2.1 XRD. The X-ray diffraction (XRD) patterns of different catalysts were obtained on a Bragg–Brentano diffract meter (Rigaku D/Max-2000) with monochromatic Cu Kα radiation (λ = 1.5418 Å). The XRD data were collected from 5 to 80° with a scan speed of 2° min^{-1}. The X-ray tube was manipulated at 40 kV and 30 mA.

2.2.2 Low temperature N_2 adsorption/desorption. The textural properties of different catalysts were measured by N_2 adsorption–desorption at liquid nitrogen temperature using an automatic analyzer (NOVA 4000, Quantachrome, USA). Before adsorption, the catalysts were degassed for 4 h at 300 °C. The specific surface areas of the samples were calculated using the Brunauer–Emmett–Teller (BET) method. The pore structural data were analyzed by the BJH (Barrett–Joyner–Halenda) method using Halsey equation for multilayer thickness.

2.2.3 FESEM. The morphologies of different catalysts were examined by a field emission scanning electron microscopy (FESEM, HITACHI S-4800) operated at 5.0 kV.

2.2.4 TEM. The transmission electron microscopy (TEM) images of different catalysts were analyzed using a JEM-2010 microscope operated at 200 kV.

2.2.5 NH_3-TPD. The acidity of different catalysts was detected by temperature-programmed desorption of ammonia (NH_3-TPD). About 0.05 g of sample was placed into a quartz reactor between two quartz wool plugs. The sample was pretreated at 400 °C for 1 h under a dry helium flow (30 mL min^{-1}) before being cooled to 120 °C and saturated with adsorbed gas. A thermal conductivity detector (TCD) was carried out from 120 to 800 °C with an increasing rate of 10 °C min^{-1} to record NH_3-TPD profile.

2.2.6 H_2-TPR. The temperature-programmed reduction (TPR) for different catalysts was measured in a programmable

temperature system. Prior to the analysis, the sample (0.2 g) was treated by dry argon (15 mL min^{-1}) at 500 °C for 1 h and then the baseline was stabilized at 25 °C for 60 min. Subsequently, the quartz reactor was heated by a mixed flow of 10% H_2 in Ar from room temperature to 950 °C with a heating rate of 10 °C min^{-1}. Finally, a TCD cell was employed to monitor and record the consumption profiles of H_2.

2.2.7 XPS. The X-ray photoelectron spectra (XPS) of different catalysts were recorded on Perkin-Elmer PHI 5000C ESCA using Al Kα radiation. All the samples were reduced in a hydrogen flow at 580 °C for 2.5 h. The binding energies (BE) were calibrated using the C1s level at 284.8 eV as an internal standard.

2.2.8 TPO. Temperature-programmed oxidation (TPO) experiments for the spent catalysts were conducted in a programmable temperature system. Prior to TPO analysis, the spent catalyst (0.05 g) was purged in flowing N_2 (15 mL min^{-1}) at 500 °C for 1 h. Then, the temperature was lowered to 40 °C to steady the baseline. Subsequently, the reactor was heated by a mixed gas flow of 10% O_2 in He from room temperature to 800 °C at the rate of 10 °C min^{-1}. Finally, a thermal conductivity detector (TCD) cell was used to determine CO_2.

2.2.9 TG. Thermogravimetric analysis was used to determine the coke content on the spent catalysts with a LCT thermogravimetric analyzer (DTG-60H), which was conducted from room temperature to 800 °C at a rising rate of 20 °C min^{-1} in a 5% O_2–95% He mixed flow (30 mL min^{-1}).

2.3 Propane dehydrogenation reaction

The propane dehydrogenation reactions were performed in a quartz fix-bed reactor (8 mm in diameter). The catalyst (0.2 g) was placed into the center of reactor, and the feed gas including C_3H_8 and Ar (C_3H_8/Ar molar ratio = 1 : 19, WHSV = 0.6 h^{-1}) was fed to the reactor. The propane dehydrogenation reactions were carried out at 620 °C and atmosphere pressure. A gas chromatography (GC, SP-6890) equipped with a flame ionization detector (FID) and an AT-PLOTPORA-Q capillary column was employed to analyze the gas compositions. The propane conversion and propylene selectivity were calculated by formulas as:

$$C_3H_8 \text{ conversion} = C_3H_{8in} - C_3H_{8out}/C_3H_{8in} \quad (1)$$

$$C_3H_6 \text{ selectivity} = C_3H_{6out}/(C_3H_{8in} - C_3H_{8out}) \quad (2)$$

where C_3H_{8in} and C_3H_{8out} are the propane content in feed and exit steams respectively; C_3H_{6out} is the propylene content in exit steam.

3 Results and discussion

3.1 Textural properties

To evaluate the textural properties of catalysts, the low-temperature N_2-physisorption isotherms were conducted and shown in Fig. 1(a) and (b). All the $x$$Ga_2O_3$/SBA-15 and 5$Ga_2O_3$/$Al_2O_3$ catalysts exhibit typical type IV adsorption isotherm with a H1-type hysteresis loop as defined by IUPAC, implying the

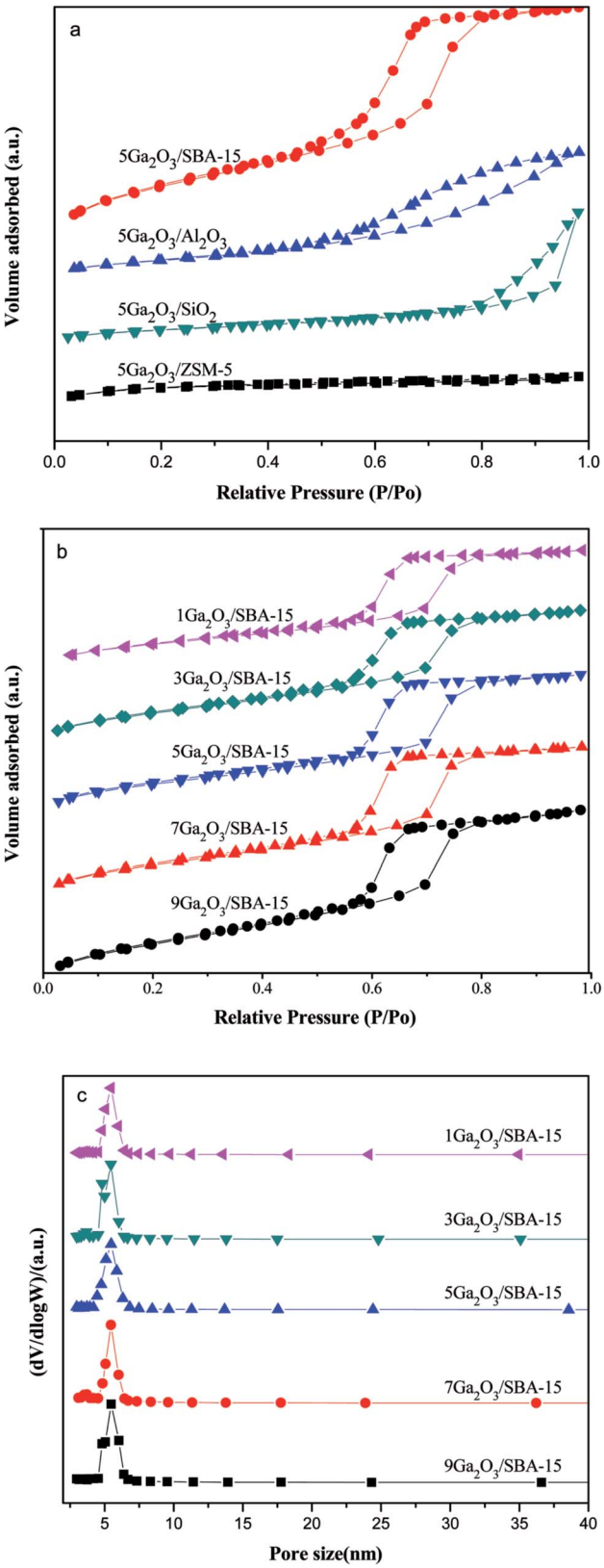

Fig. 1 (a) and (b) Low temperature N_2 adsorption–desorption isotherms of $x$$Ga_2O_3$/SBA-15, 5$Ga_2O_3$/$Al_2O_3$, 5$Ga_2O_3$/$SiO_2$, 5$Ga_2O_3$/ZSM-5 catalysts and (c) the corresponding pore size distributions of $x$$Ga_2O_3$/SBA-15 catalysts.

presence of mesoporous structure. Moreover, the isotherms of xGa$_2$O$_3$/SBA-15 catalysts show comparatively sharp step with the increase of relative pressure (P/P_0) as compared with that of 5Ga$_2$O$_3$/Al$_2$O$_3$ sample. According to the previous studies,[34] this is the characteristic of capillary condensation of nitrogen in ordered mesopores. The low-temperature N_2-physisorption isotherm for 5Ga$_2$O$_3$/ZSM-5 is also illustrated in Fig. 1(a). It shows type I adsorption isotherm with a plateau at higher relative pressure in accordance with the microporous nature of limited mesoporosity of the samples (BDDT classifications[31]). Furthermore, the type H3 (according to IUPAC) hysteresis loop can be noticed for 5Ga$_2$O$_3$/SiO$_2$ sample, which often corresponds with the slit-shaped pores.[35] The textural properties of the different catalysts are listed in Table 1. As can be seen, the specific surface areas of all the catalysts are mainly determined by the support materials. From Table 1, the specific surface area (S_{BET}) values of different Ga$_2$O$_3$-based catalysts are in the following sequence: SBA-15 > ZSM-5 > Al$_2$O$_3$ > SiO$_2$. As regards xGa$_2$O$_3$/SBA-15 catalysts in Fig. 1(b), with the increase of gallium oxide loading from 1 wt% to 9 wt%, the S_{BET} and pore volume (V_p) notably decrease, implying that gallium species might penetrate into the mesoporous channels of SBA-15 and lead the channels to be partially blocked. Moreover, as exhibited in Fig. 2(c), the pore size distributions of xGa$_2$O$_3$/SBA-15 catalysts are measured by the BJH model according to the desorption branches of the isotherms, and the pore diameter (D_p) varies little with the increase of Ga$_2$O$_3$ addition.

3.2 XRD

The XRD patterns of the different catalysts are depicted in Fig. 2. Apparently, the characteristic peaks of the corresponding supports are found for all the samples, indicating that the original structure of the support is not destroyed during the catalyst preparation process. In addition, in the wide-angle region (Fig. 2(a)), these materials do not exhibit the characteristic peaks of Ga$_2$O$_3$ crystalline phases, probably due to their small particle size and/or low concentration below XRD detection limitation. Moreover, the low-angle XRD patterns of xGa$_2$O$_3$/SBA-15 samples are depicted in Fig. 2(b). As can be seen, the unique diffraction planes of (100), (110) and (200) are ascribed to the ordered two-dimensional hexagonal mesoporous structures, and the diffraction peaks of mesoporous structure vary little with the increase of Ga$_2$O$_3$ content from 1 to 5 wt%. As the Ga$_2$O$_3$ loading further increases to 7 wt% and 9 wt%, the peak intensity of (100) diffraction plane decreases significantly, and the peak moves to smaller angle location, suggesting that the introduction of overhigh Ga$_2$O$_3$ weakens the degree of long-range order of SBA-15.[36,37]

Table 1 Textural properties of the different catalysts

Samples	S_{BET} ($m^2\ g^{-1}$)	V_p ($cm^3\ g^{-1}$)	D_p (nm)
5Ga$_2$O$_3$/ZSM-5	327	0.21	—
5Ga$_2$O$_3$/Al$_2$O$_3$	195	0.45	5.06
5Ga$_2$O$_3$/SiO$_2$	137	0.42	11.5
1Ga$_2$O$_3$/SBA-15	721	1.00	5.47
3Ga$_2$O$_3$/SBA-15	661	0.93	5.46
5Ga$_2$O$_3$/SBA-15	628	0.86	5.48
7Ga$_2$O$_3$/SBA-15	623	0.85	5.46
9Ga$_2$O$_3$/SBA-15	556	0.77	5.46

3.3 FESEM and TEM

The FESEM images of the different catalysts are presented in Fig. 3. As can be seen, the FESEM image of 5Ga$_2$O$_3$/ZSM-5 sample reveals highly crystalline zeolites of prismatic structure. In the cases of xGa$_2$O$_3$/SBA-15, they all show bound worm-like feature with a relatively uniform size of about 1 μm. However, with the increase of Ga$_2$O$_3$ content from 1 wt% to 9 wt%, the long-range worm-like morphology becomes chaos, and the order degree of structure declines. It can be explained that the increase of Ga$_2$O$_3$ content leads to the collapse of molecular sieve structure.

The ordered porous structures of 5Ga$_2$O$_3$/ZSM-5 and xGa$_2$O$_3$/SBA-15 samples were further observed by TEM. The images are collected and showed in Fig. 4. From the TEM image of 5Ga$_2$O$_3$/ZSM-5 sample, the well-ordered lattice fringes are clearly distinguished in the high-magnification image, which

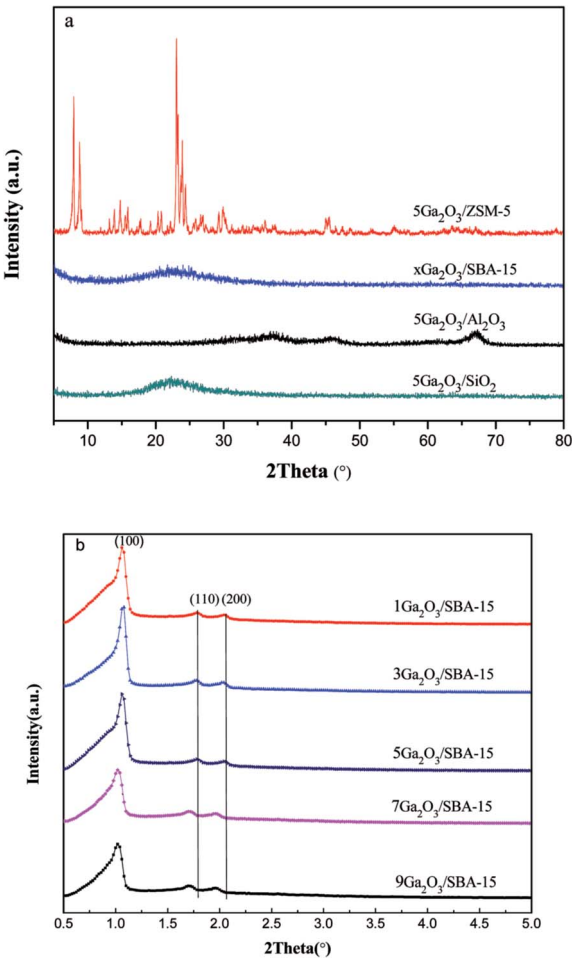

Fig. 2 (a) Wide-angle X-ray diffraction patterns of the different catalysts and (b) small-angle X-ray diffraction pattern of xGa$_2$O$_3$/SBA-15 catalyst.

demonstrates the high crystallinity of ZSM-5. As for $x$$Ga_2O_3$/SBA-15 samples, the micrographs reveal the presence of well-ordered hexagonal arrays of mesoporous channels. However, as loading content increases to 9 wt%, less regular channels are observed from Fig. 4(f). These TEM images are in good agreement with the XRD, BET and SEM results. Furthermore, as indicated by the arrows, the agglomerated gallium species can also be noticed on $7Ga_2O_3$/SBA-15 and $9Ga_2O_3$/SBA-15 catalysts, which implies that the dispersion of Ga species is not highly homogeneous under high loading concentration.

3.4 NH_3-TPD

The acidity of different catalysts was probed by temperature-programmed desorption of ammonia method, and the corresponding NH_3-TPD curves are displayed in Fig. 5. The semi-quantitative analysis is achieved by deconvoluting the peaks using Gaussian curve fitting method. The calculated results containing total acidity and acidity strength distribution are summarized in Table 2. It is clear that $5Ga_2O_3$/ZSM-5 catalyst exhibits two ammonia desorption peaks. The first peak centered (peak I) at ~220 °C is attributed to the weak acid sites; while the second peak centered (peak II) at ~420 °C is attributed to the strong acid sites.[38] Furthermore, the largest strong acid sites also can be observed over Ga_2O_3/ZSM-5 catalyst. From Fig. 5 and Table 2, it can be seen that nearly half of total acidity is ascribed to strong acid sites for $5Ga_2O_3$/ZSM-5 catalyst. As regards the $5Ga_2O_3/Al_2O_3$ catalyst, it displays three desorption peaks, a broad desorption peak (peak I) centered at ~190 °C with a shoulder (peak II) at higher temperatures ~270 °C and a peak (peak III) with a maximal temperature (TM) centered at ~480 °C. It is generally accepted that these three desorption peaks are ascribed to be weak, medium and strong acid sites respectively.[39] In comparison with $5Ga_2O_3$/ZSM-5 and $5Ga_2O_3/Al_2O_3$ catalysts, the ammonia desorption peaks almost cannot be visible over $x$$Ga_2O_3$/SBA-15 and $5Ga_2O_3/SiO_2$ samples. This phenomenon may be attributed to the inherent nature of pure silicon support. From Table 2, though the $x$$Ga_2O_3$/SBA-15 catalysts possess the very weak surface acidity, the acid properties still have some changes with the increase of Ga_2O_3 content. The $5Ga_2O_3$/SBA-15 and $7Ga_2O_3$/SBA-15 samples show relatively high total acidity and weak to medium strong acid sites as compared with those of other three samples, but the change of the amount of strong acid sites is not obvious. The previous studies demonstrated that undesirable side reactions were easily initiated by the strong acid sites of catalysts.[40] By inference, the undesirable side reactions may easily occur over $5Ga_2O_3$/ZSM-5 catalyst.

3.5 H_2-TPR

To determine the effects of different supports and loading amount on the reduction properties, H_2-TPR technique was implemented, and the curves of the corresponding fresh

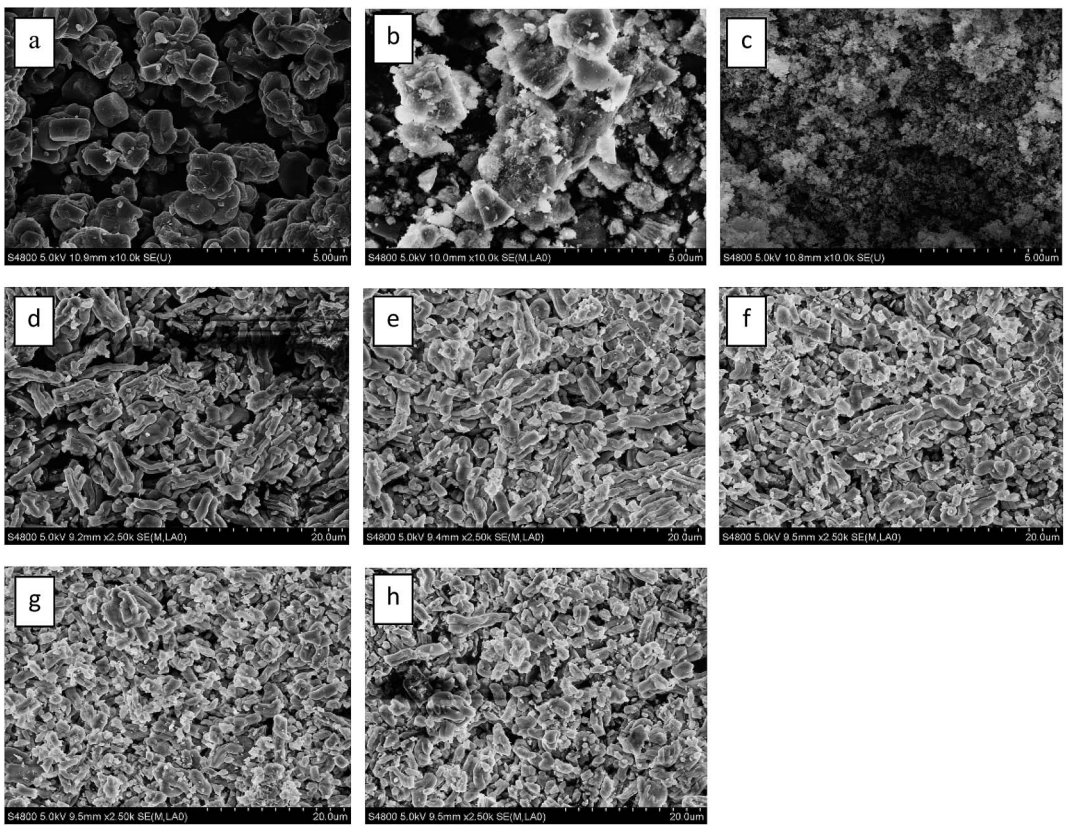

Fig. 3 FESEM images of (a) $5Ga_2O_3$/ZSM-5; (b) $5Ga_2O_3/Al_2O_3$; (c) $5Ga_2O_3/SiO_2$; (d) $1Ga_2O_3$/SBA-15; (e) $3Ga_2O_3$/SBA-15; (f) $5Ga_2O_3$/SBA-15; (g) $7Ga_2O_3$/SBA-15; (h) $9Ga_2O_3$/SBA-15.

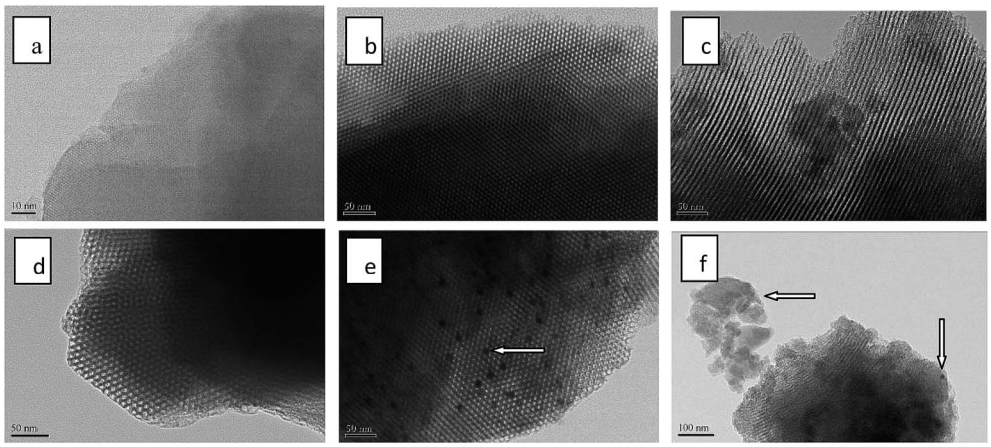

Fig. 4 TEM micrographs of (a) $5Ga_2O_3$/ZSM-5; (b) $1Ga_2O_3$/SBA-15; (c) $3Ga_2O_3$/SBA-15; (d) $5Ga_2O_3$/SBA-15; (e) $7Ga_2O_3$/SBA-15; (f) $9Ga_2O_3$/SBA-15.

catalysts are illustrated in Fig. 6(a). The semi-quantitative H_2 consumption is summarized in Table 3, which is obtained by fitting the H_2-TPR curves using the Gaussian deconvolution method. It can be seen that all the catalysts present two reduction consumption peaks at about 600 °C (peak I) and 900 °C (peak II). As reported previously,[26] the peak I is ascribed to the reduction of well-dispersed Ga species, such as micro Ga_2O_3 particles and/or GaO^+ species interacting with the support, and the peak II can be assigned to bulk Ga_2O_3 particles and the loosely supported part of Ga_2O_3, respectively. In the case of $5Ga_2O_3$/ZSM-5, the strongest reduction peak I and the weakest reduction peak II can be observed, implying that the incorporated Ga species of $5Ga_2O_3$/ZSM-5 catalyst are mostly retained as well-dispersed Ga species. The analysis shows that compared with $5Ga_2O_3$/ZSM-5 catalyst, a weaker reduction peak I and slightly stronger reduction peak II can be observed over the $5Ga_2O_3/Al_2O_3$ catalyst, suggesting that the amount of well-dispersed Ga species on $5Ga_2O_3/Al_2O_3$ catalyst is less than that of $5Ga_2O_3$/ZSM-5 catalyst. This phenomenon should be highly related to the acidic properties of catalysts. As shown in Table 4, the ratio of well-dispersed Ga in $5Ga_2O_3$/ZSM-5 to $5Ga_2O_3/Al_2O_3$ is approximately equal to that of the strong acid peak area in the corresponding samples. This similar phenomenon was also mentioned by Ausavasukhi *et al.*[25] In addition, a small peak at about 690 °C can be noticed, which should be attributed to the reduction of OH groups or Al of alumina support.[41] On the other hand, Fig. 6(b) shows the TPR curves of $x$$Ga_2O_3$/SBA-15 catalysts. It can be seen that all the samples also display similar two peaks, a small shoulder peak at lower temperature and intensive one at very high temperature even over 950 °C. More specifically, the hydrogen consumption areas of peak II over $x$$Ga_2O_3$/SBA-15 catalysts increase as the Ga_2O_3 content increases. The $5Ga_2O_3$/SBA-15 catalyst exhibits the strongest signal value among all the catalysts, which indicates that the $5Ga_2O_3$/SBA-15 sample possesses the largest amount of well-dispersed Ga species. Furthermore, for all the $x$$Ga_2O_3$/SBA-15 catalysts, the peak intensity at about 600 °C is much weaker than those of $5Ga_2O_3$/ZSM-5 and $5Ga_2O_3/Al_2O_3$ catalysts. This phenomenon can be explained that the low acidity of $x$$Ga_2O_3$/SBA-15 catalysts is adverse to the dispersion of Ga species. As for the TPR curve of $5Ga_2O_3/SiO_2$ sample, two weak reduction peaks for Ga species can be found, which means that the SiO_2 support is hard to stabilize small Ga_2O_3 particles or GaO^+ species. It is very unfavorable to the reaction. The similar results were also mentioned in previous reports.[42,43]

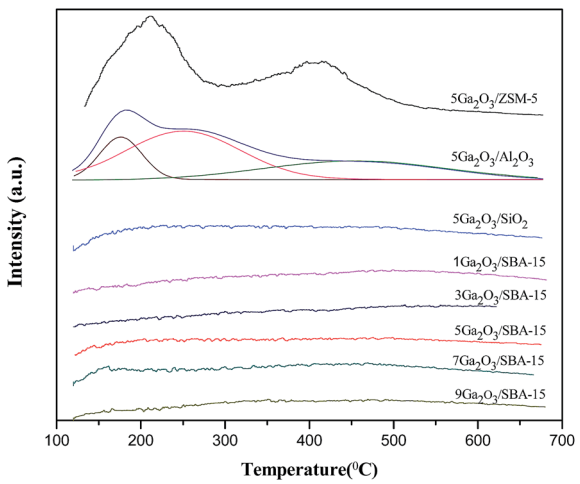

Fig. 5 NH_3-TPD profiles of the different catalysts.

Table 2 The semi-quantitative results of NH_3-TPD measurements

Catalysts	TM (°C)			Total area (a.u.)	Peak area fraction (%)	
	I	II	III		I + II	III
$5Ga_2O_3$/ZSM-5	220	—	420	399	53.4	46.6
$5Ga_2O_3/Al_2O_3$	190	270	480	403	67.3	32.7
$5Ga_2O_3/SiO_2$	218	314	495	69.2	34.5	65.5
$1Ga_2O_3$/SBA-15	198	320	502	51.4	15.8	84.2
$3Ga_2O_3$/SBA-15	206	316	513	48.6	13.4	86.6
$5Ga_2O_3$/SBA-15	200	301	460	60.8	27.8	72.2
$7Ga_2O_3$/SBA-15	180	318	455	53.2	23.2	76.8
$9Ga_2O_3$/SBA-15	179	301	486	49.3	18.3	81.7

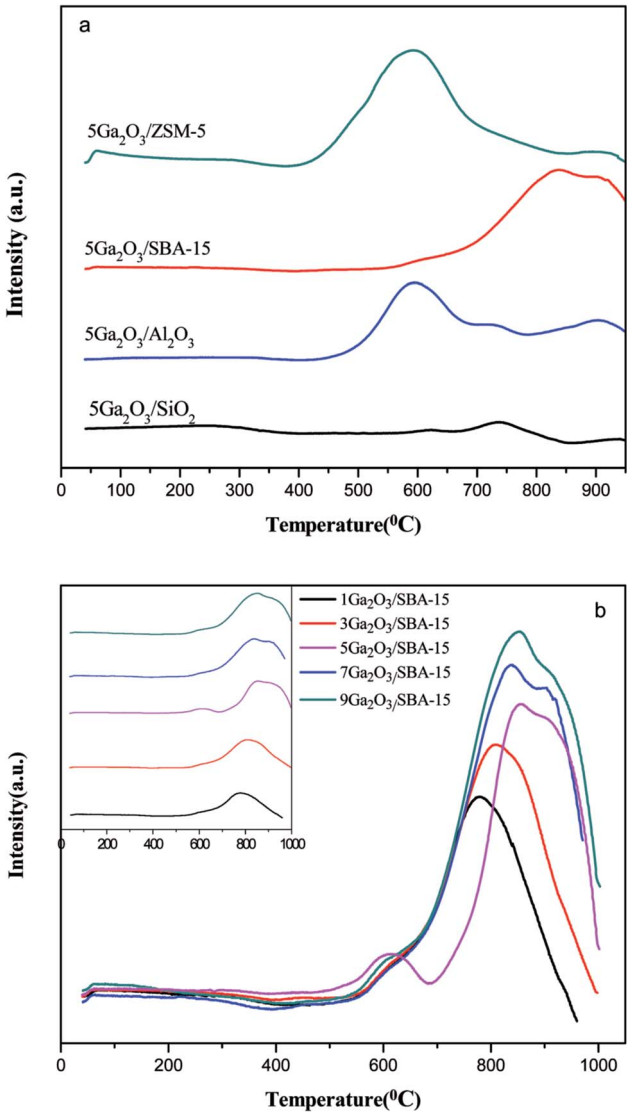

Fig. 6 H_2-TPR profiles of the different catalysts.

3.6 XPS

To further elucidate the chemical state of Ga species, XPS analyses were measured. The XPS spectra and semi-quantitative results of various catalysts are shown in Fig. 7 and Table 5 respectively. As can be seen in Fig. 7, $5Ga_2O_3$/ZSM-5 and $5Ga_2O_3/Al_2O_3$ catalysts present three peaks at ~25 eV (peak I), ~21 eV (peak II) and ~19.8 eV (peak III) similar to the previous literatures.[16,44,45] The high binding energy (~25 eV) is ascribed to O2s band; the binding energy (~21 eV) is assigned to Ga3d band, and the low energy peak at ~19.8 eV is attributed to $Ga^{\delta+}$ species ($\delta < 2$).[45] From Table 5, the percentages of $Ga^{\delta+}$ species ($\delta < 2$) for $5Ga_2O_3$/ZSM-5 and $5Ga_2O_3/Al_2O_3$ catalysts are about 62% and 11% respectively, implying that partial Ga_2O_3 is reduced on these two supports during the catalyst preparation process. The similar viewpoint was also reported in the previous literature.[46] As for xGa_2O_3/SBA-15 and $5Ga_2O_3/SiO_2$ catalysts, there are two deconvoluted peaks (peak I and peak II). The fraction of gallium in the oxidized state for xGa_2O_3/SBA-15 catalyst increases with the increase of Ga_2O_3 content from 1 to 9 wt%. Moreover, it can be seen from Table 5 that the Ga3d banding energy of the gallium species in the Ga_2O_3/SiO_2 is reduced by 0.5 as compared with those in the other three samples. It is remarkable that the Ga3d banding energy of the gallium species in pure β-Ga_2O_3 is the same as that in $5Ga_2O_3/SiO_2$ catalyst,[44] indicating that using ZSM-5, Al_2O_3 and SBA-15 supports can strengthen the interaction between Ga species and support. The similar conclusion was also reported by Xu *et al.*[18] These results imply that the different supports can play a significant role in determining the chemical state of Ga species.

Table 3 The semi-quantitative H_2-TPR results for the different catalysts

Catalysts	Total area (a.u.) ($\times 10^4$)	Peak I area (a.u.) ($\times 10^4$)	Peak II area (a.u.) ($\times 10^4$)
$5Ga_2O_3$/ZSM-5	1.60	1.38	0.22
$5Ga_2O_3$/SBA-15	1.34	0.05	1.29
$5Ga_2O_3/Al_2O_3$	1.41	0.99	0.42
$5Ga_2O_3/SiO_2$	0.05	0.01	0.04

3.7 Catalytic performances

3.7.1 Effect of different supports. The catalysts with different supports were subjected to the propane dehydrogenation reaction for 30 h. The propane conversion and propylene selectivity are displayed in Fig. 8. As can be seen, the initial conversions of propane for different catalysts decrease in the following order: $5Ga_2O_3$/ZSM-5 > $5Ga_2O_3/Al_2O_3$ > $5Ga_2O_3$/SBA-15 > $5Ga_2O_3/SiO_2$. The $5Ga_2O_3$/ZSM-5 catalyst shows the highest initial propane conversion (78.1%), which is much higher than those of the other samples. However, the worst stability of $5Ga_2O_3$/ZSM-5 catalyst is found among all the samples. The final propane conversion is only 11.5%. As regards the $5Ga_2O_3$/SBA-15 sample, although the initial conversion of propane is 29.7%, it exhibits the highest catalytic stability. The final propane conversion still attains 21.4% after 30 h of propane dehydrogenation reaction. When the Al_2O_3 is chosen as the support, the relatively high initial propane conversion (46.0%) over $5Ga_2O_3/Al_2O_3$ can be obtained, but the quick deactivation of this sample is also observed, and the final conversion value is only 5.3%. For the $5Ga_2O_3/SiO_2$ catalyst, a low and stable propane conversion (around 5.5%) can be observed. The TOF values of different catalysts at 20 h are calculated and included

Table 4 The relationship between the reduction properties and the strong acid sites on the different supports

	$5Ga_2O_3$/ZSM-5	$5Ga_2O_3/Al_2O_3$	Area ratio
H_2-TPR peak I area (a.u.)	1.38	0.99	1.39
NH_3-TPD peak III area (a.u.)	185.93	131.78	1.41

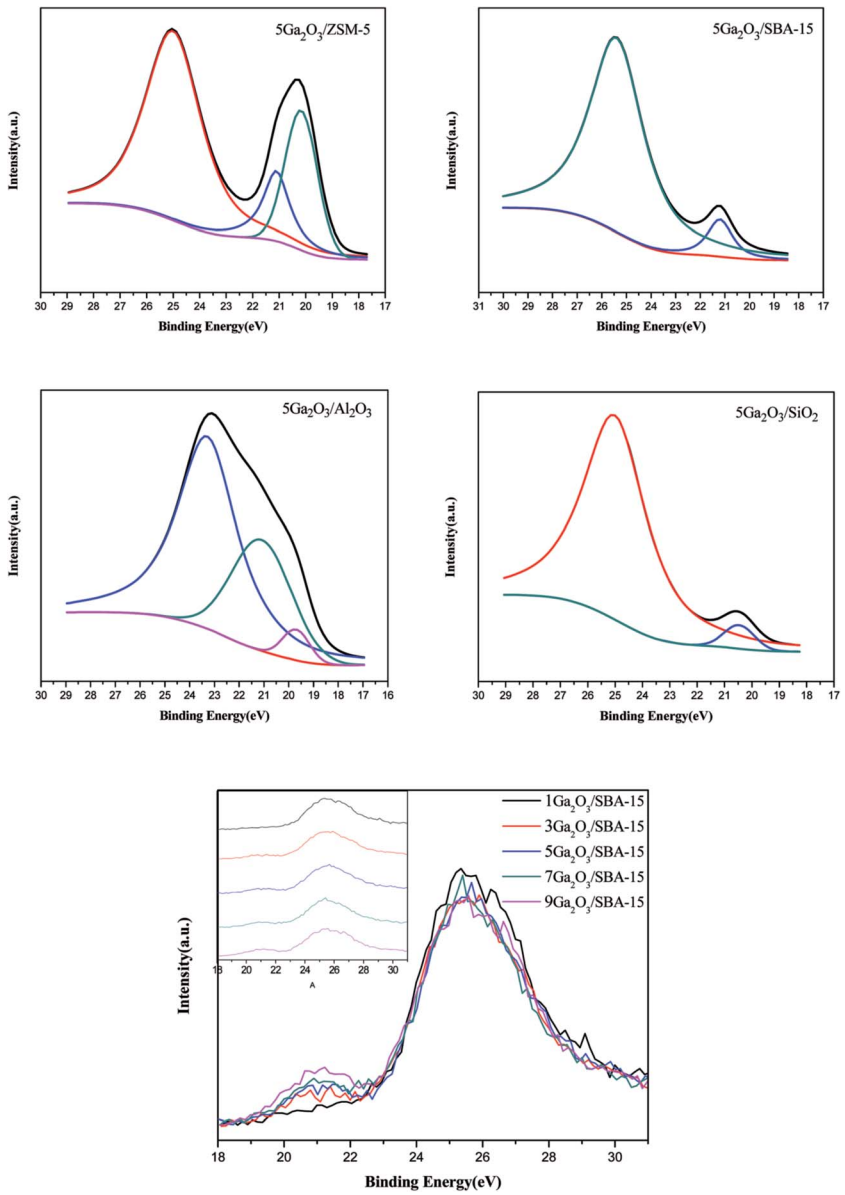

Fig. 7 Ga3d XPS spectra of the different catalysts.

in Table 6. It is remarkable that the TOF values show the similar variation regularity to that of propane conversion over the corresponding catalysts. The highest TOF value can be found over $5Ga_2O_3$/SBA-15 catalyst, indicating that it displays the high dehydrogenation efficiency of Ga species.

From Fig. 8, it can be seen that the propylene selectivity exhibits an apparent rise of for $5Ga_2O_3$/ZSM-5 catalyst in the initial several hours and then gradually stabilizes at around 89% after 8 h reaction. The $5Ga_2O_3/Al_2O_3$ catalyst presents the highest initial propylene selectivity, and slightly decreases from 95.8% to 85.1% after 30 h reaction. The propylene selectivity for $5Ga_2O_3$/SBA-15 catalyst attains about 92.0% and varies little in the whole 30 h reaction period. As for the $5Ga_2O_3/SiO_2$ sample, a relatively low propylene selectivity of around 86% is observed.

The variation of the catalytic performances can be explained as following. In general, for Ga_2O_3-supported catalysts, there are three kinds of active centers in the fresh catalysts: well-dispersed Ga species, GaO^+ and bulk Ga_2O_3.[25,47] The well-dispersed Ga species and GaO^+ usually have higher dehydrogenation activity as compared with bulk Ga_2O_3.[25] It can be seen from the H_2-TPR curves in Fig. 6 that the initial catalytic activities of different catalysts are in good agreement with the amount of well-dispersed Ga species of the corresponding catalysts. Furthermore, the TEM images also certify the existence of bulk Ga_2O_3 in $7Ga_2O_3$/SBA-15 and $9Ga_2O_3$/SBA-15 samples. Secondly, the researchers reported that the reduced gallium ions ($Ga^{\delta+}$ cations, $\delta < 2$) were considered to be a reason for the high activity, and monovalent Ga was regarded as the second most active species.[25,47,48] As shown in Fig. 7 and Table 5, the content of the reduced gallium species on $5Ga_2O_3$/ZSM-5 catalyst and $5Ga_2O_3/Al_2O_3$ catalyst are 62% and 11% respectively. Nevertheless, the reduced gallium species cannot be

Table 5 The semi-quantitative XPS results for the different catalysts

Catalysts	Ga3d binding energy (eV)	Ga^{3+} (%)	$Ga^{\delta+a}$ (%)
$5Ga_2O_3/ZSM\text{-}5$	21.0/19.8	38	62
$xGa_2O_3/SBA\text{-}15$	21.0	100	0
$5Ga_2O_3/Al_2O_3$	21.0/19.8	89	11
$5Ga_2O_3/SiO_2$	20.5	100	0

[a] $\delta < 2$.

found over the other two pure silica supported catalysts. In this sense, this is another reasonable explanation for the much better catalytic performance of $5Ga_2O_3/ZSM\text{-}5$ than the other three catalysts. Thirdly, as shown in Table 5, the weak interaction between Ga species and SiO_2 support is found for $5Ga_2O_3/SiO_2$ sample, but the other three catalysts exhibit the strong interactions between Ga species and the supports. This may be the reason why $5Ga_2O_3/SiO_2$ catalyst possesses the lowest catalytic activity. Finally, according to the textural parameters in Fig. 1 and Table 1, the relatively high surface area and unique structure of ZSM-5 support may be responsible for the relatively high catalytic activity of $5Ga_2O_3/ZSM\text{-}5$ catalyst.

As for the changes of propylene selectivity, it is well-known that the strong acid sites generally promote the deep dehydrogenation due to isomerization and coking reactions on the surfaces of catalysts. Aromatization of propylene would also take place on the Brønsted acid sites of supports. All these factors will lower propylene selectivity.[49] Moreover, not only the surface acidic properties of support but also the active components can give rise to the variation of propylene selectivity. The previous study has proved that the dihydrogen molecule is dissociatively adsorbed on gallium oxide on the catalyst surface, which may cause the occurrence of hydrogenolysis reaction.[50] With regards to $5Ga_2O_3/ZSM\text{-}5$ sample, the lowest selectivity in the initial hours must be related to the strong acidity sites and well-dispersed Ga species, which results in more side reactions (Fig. 9). Meantime, there also exist the relatively high selectivities to methane and ethane (Fig. 9), implying the occurrence of hydrogenolysis reaction, and the following increased selectivity should be due to the cover of acid sites by coke deposits. For the $5Ga_2O_3/Al_2O_3$ catalyst, the NH_3-TPD results (Fig. 5) show that the strong acid sites are relatively suitable, and thus the undesired side reactions can be suppressed. The $5Ga_2O_3/SBA\text{-}15$ and $5Ga_2O_3/SiO_2$ samples possess the relatively high propylene selectivity values among all the samples, which are consistent with the extremely weak acidity.

3.7.2 Effect of Ga_2O_3 content. The catalytic performances over $xGa_2O_3/SBA\text{-}15$ catalysts with different Ga_2O_3 content are illustrated in Fig. 10. It can be observed that $5Ga_2O_3/SBA\text{-}15$ sample shows the highest conversion, selectivity and catalytic stability, which has the initial propane conversion and final one of 31.7% and 30.3%. However, the higher or lower Ga_2O_3 loading amount both leads to a decline of initial propane conversion. $1Ga_2O_3/SBA\text{-}15$ sample exhibits the lowest catalytic activity among all the catalysts. The TOF values of $xGa_2O_3/SBA\text{-}15$ are also shown in Table 6. It can be seen that $1Ga_2O_3/SBA\text{-}15$ sample has the highest TOF value, which should be ascribed to the high Ga species dispersion under the minimum Ga_2O_3 loading. As for the other samples, the TOF values first increase, and then decrease with the increase of the amount of gallium oxide, and the $5Ga_2O_3/SBA\text{-}15$ sample possesses the second highest TOF value. This phenomenon can be probably attributed to the formation of bulk Ga_2O_3, which leads to the decline of dehydrogenation efficiency of gallium oxide.

From Fig. 10, $5Ga_2O_3/SBA\text{-}15$ catalyst presents the highest propylene selectivity among all the samples. $1Ga_2O_3/SBA\text{-}15$ and $9Ga_2O_3/SBA\text{-}15$ catalysts show the relatively lower propylene selectivities. Also, it is found that the propylene selectivity has the similar variation trend to propane conversion with regard to the Ga_2O_3 content for $xGa_2O_3/SBA\text{-}15$ catalysts.

The catalytic performances over the synthesized catalysts with different loadings can be explained as following. According

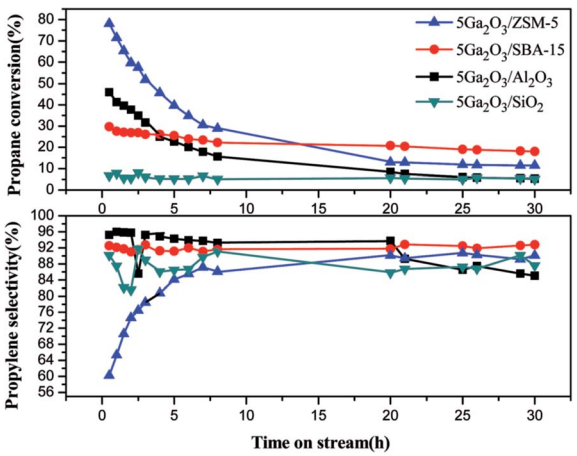

Fig. 8 Propane conversion and propylene selectivity of the different catalysts as a function of time (reaction conditions: T = 620 °C; C_3H_8 : Ar (molar ratio) = 1 : 19; WHSV = 0.6 h^{-1}; $m_{cat.}$ = 0.2 g).

Table 6 Amounts of coke on the spent different supported and $xGa_2O_3/SBA\text{-}15$ catalysts for propane dehydrogenation after 30 h and 2 h reaction respectively, and TOF values of the different catalysts[a]

Samples	Coke amount[b] (%)	TOF (s^{-1}) ($\times 10^{-2}$)
$5Ga_2O_3/ZSM\text{-}5$[c]	12.6	1.81
$5Ga_2O_3/SBA\text{-}15$[c]	4.55	2.91
$5Ga_2O_3/Al_2O_3$[c]	2.86	1.16
$5Ga_2O_3/SiO_2$[c]	0.96	0.80
$1Ga_2O_3/SBA\text{-}15$[d]	3.97	6.92
$3Ga_2O_3/SBA\text{-}15$[d]	5.85	3.72
$5Ga_2O_3/SBA\text{-}15$[d]	3.11	4.20
$7Ga_2O_3/SBA\text{-}15$[d]	6.32	2.08
$9Ga_2O_3/SBA\text{-}15$[d]	6.52	1.64
SBA-15	0.82	—

[a] Note: the coke on the SBA-15 and the Ga_2O_3 catalysts supported on various supports was measured after 30 h of propane dehydrogenation reaction; the coke on the $xGa_2O_3/SBA\text{-}15$ was measured after 2 h of propane dehydrogenation reaction. [b] Experimental value calculated from thermogravimetric (TG) analysis. [c] C_3H_8 turn frequency (TOF) in the 20 h reaction. [d] C_3H_8 turn frequency (TOF) in the 2 h reaction.

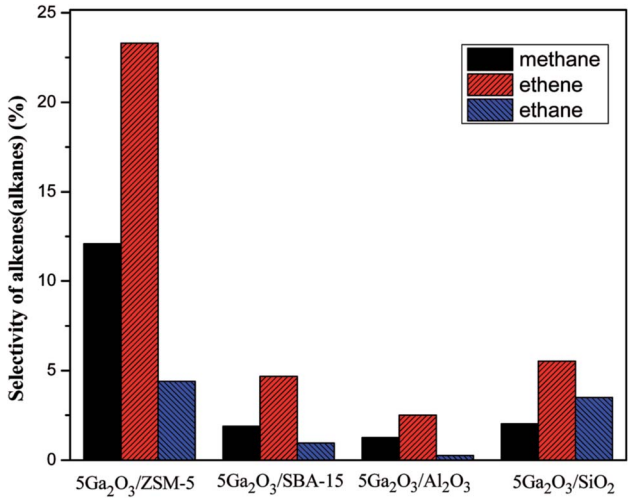

Fig. 9 Selectivities to alkanes (alkenes) over the different catalysts in the initial 30 min reaction: (reaction conditions: $T = 620$ °C; C_3H_8 : Ar (molar ratio) = 1 : 19; WHSV = 0.6 h^{-1}; $m_{cat.} = 0.2$ g).

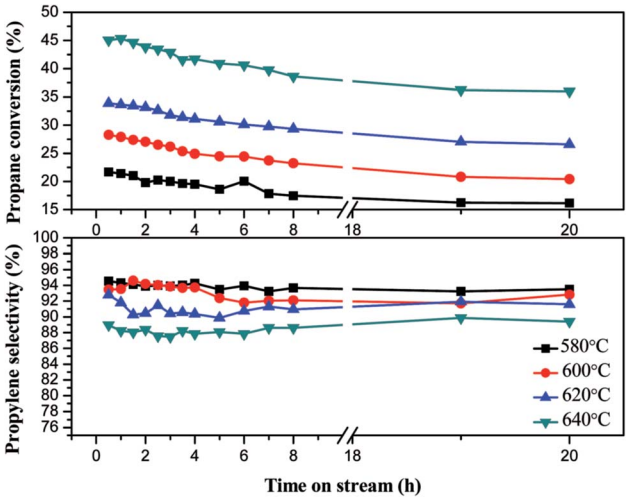

Fig. 11 The effect of reaction temperature on the performance of $5Ga_2O_3$/SBA-15 catalyst in propane dehydrogenation.

to XRD, BET, SEM and TEM results, the high Ga_2O_3 content can block the pores of SBA-15, destroy the structural integrity of SBA-15 and lead to the formation of bulk Ga species on the support. The H_2-TPR curves in Fig. 6(b) also verify that more well-dispersed Ga species exist on $5Ga_2O_3$/SBA-15 sample, which is in coincidence with the best catalytic performance. Furthermore, as shown in Table 2, the catalytic performances of xGa_2O_3/SBA-15 catalysts are closely related to the variation of the total acid of the catalysts with respect to Ga_2O_3 content. It is notable that the strong acid sites of xGa_2O_3/SBA-15 catalysts almost vary little with the increase of Ga_2O_3 content, and all the catalysts have the similar amounts of well-dispersed Ga species, implying that the influence of the amount of well-dispersed Ga species is mostly related to the acidity rather than the loading content of Ga_2O_3. When Ga content increases, the Ga species begin to enrich in the form of large Ga_2O_3 clusters rather than well-dispersed species. Ausavasukhi *et al.*[43] also reported a similar conclusion.

3.7.3 Effect of reaction temperature. Fig. 11 shows the effect of reaction temperature on the performance of $5Ga_2O_3$/SBA-15 catalyst in propane dehydrogenation. The initial propane conversions of 21.7%, 28.3%, 33.8% and 45.0% are obtained at 580, 600, 620 and 640 °C respectively, and they decrease to 16.1%, 20.4%, 26.6% and 36.0% after 20 h reaction. The initial propylene selectivities are 94.5%, 93.5%, 92.8% and 90% at 580, 600, 620 and 640 °C respectively. The decreased selectivity with the increase of temperature can be ascribed to the side reactions like thermal cracking *etc.* Though the highest propane conversion is achieved at 640 °C at the expense of the lowest selectivity, it is not a desirable reaction parameter. Compared the results at 580 °C with others, the propylene selectivity evidently decreases at other three temperatures. However, the initial propane conversion is only 16.1% when the reaction is carried out at 580 °C. In general, the reaction

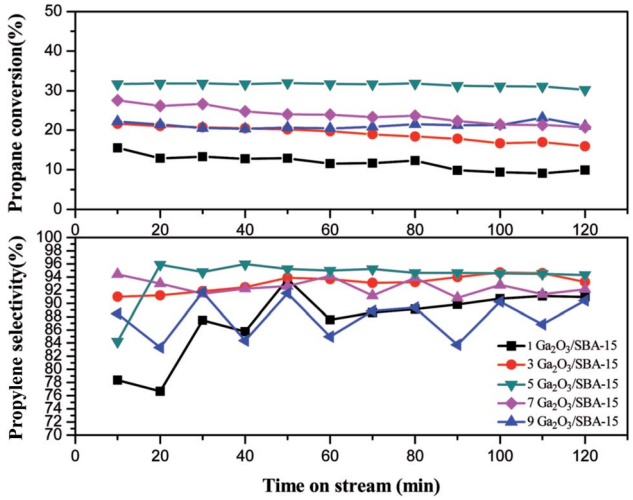

Fig. 10 The effect of Ga_2O_3 content of the catalysts on the catalytic performance in propane dehydrogenation (reaction conditions: $T = 620$ °C; C_3H_8 : Ar (molar ratio) = 1 : 19; WHSV = 0.6 h^{-1}; $m_{cat.} = 0.2$ g).

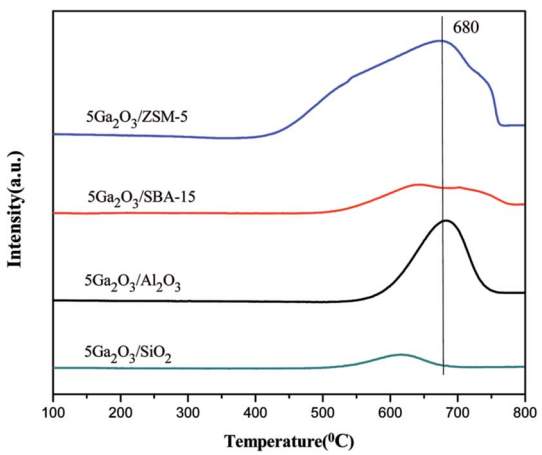

Fig. 12 TPO profiles of the spent catalysts.

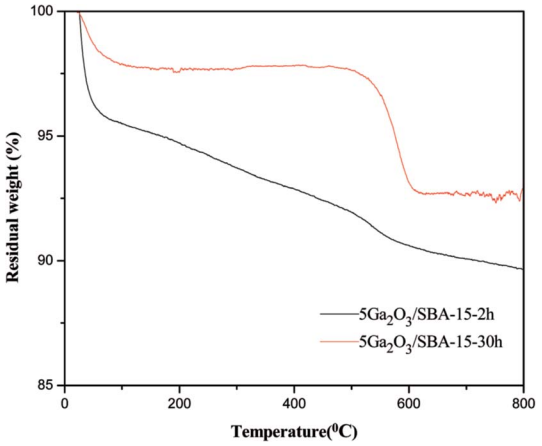

Fig. 13 TG profiles of the spent $5Ga_2O_3$/SBA-15 catalysts.

temperature at 600–620 °C should be the ideal selection to balance the conversion and selectivity of propane dehydrogenation reaction.

As mentioned above, in this work, coke is one main reason to catalyst deactivation.[51,52] The strong acidity can promote the coke deposition on the catalyst surface.[53] The total coke amounts of the spent catalysts were analyzed by TPO and TG measurements. It can be seen from Fig. 12 that all the TPO curves of the spent catalysts present one major peak,[54] which is attributed to coke combustion on the catalysts. The peak for $5Ga_2O_3/SiO_2$ sample presents a relatively lower temperature than the other three catalysts, meaning that the deposited coke is easily combusted. Coke quantitative analysis (Table 6) is in good agreement with TPO results, and the order of coke amount is as follows: $5Ga_2O_3$/ZSM-5 > $5Ga_2O_3$/SBA-15 > $5Ga_2O_3/Al_2O_3$ > $5Ga_2O_3/SiO_2$. The spent $5Ga_2O_3$/ZSM-5 catalyst has the largest coke amount (12.6%), which coincides with the propylene selectivity in Fig. 8. In this case, as discussed before (Table 2), the $5Ga_2O_3$/ZSM-5 possesses the quite strong acidity. This should be responsible for the largest amount of coke deposition. When SBA-15 material is used as the support, the second most coke amount of $5Ga_2O_3$/SBA-15 which has the low acidity may owe to the high temperature, Ga species and largest S_{BET} value. From Table 6, a small amount of coke can be found on pure SBA-15 support, implying that the propane thermal cracking reactions are inevitable during the long-term reaction at such a high reaction temperature (620°). Furthermore, the Ga_2O_3-based catalysts are known to be effective catalysts for promoting the selective conversion of light alkanes to aromatics. Many authors agree that the aromatization reaction occurs *via* a bifunctional mechanism. Not only strong acid sites but also Ga species can enhance the dehydrogenation steps, including the dehydrogenation of alkane, higher olefins, and cycloolefins. Meriaudeau illustrated that the dihydrogen molecule was dissociatively adsorbed on gallium oxide. These might result in producing a large amount of coke precursors during the process of reaction. Moreover, the mesoporous character and high S_{BET} of SBA-15 make the support have a certain pore volume, which can contain the coke easily. On the contrary, with respect to $5Ga_2O_3/\gamma$-Al_2O_3 catalyst, without high S_{BET} value, the coke deposition quickly covers the active sites, and results in an evident decrease in the catalyst activity. When SiO_2 material is used as the support, the lowest amount of coke on the $5Ga_2O_3/SiO_2$ can be found, which is well coincident with the dreadful catalytic activity.

As for xGa_2O_3/SBA-15 catalysts, the total coke amounts of the spent catalysts are also illustrated in Table 6. The $5Ga_2O_3$/SBA-15 and $9Ga_2O_3$/SBA-15 catalysts possess the lowest and highest coke content among all the samples respectively, which are in accord with the catalytic performance. Meanwhile, the different reaction time (2 h and 30 h) on the nature of coke components are also discussed. As can be seen from Fig. 13, the weight loss between 0 and 300 °C can be considered as the loss of surface water and water adsorption phase, and the weight loss between 300 and 600 °C is attributed to the coke combustion on the catalyst surface. It should be noted that the weight loss trend of

Table 7 Comparison of the catalytic performances of different catalysts for propane dehydrogenation reaction

Catalysts	Ga_2O_3 content (wt%)	T (°C)	WHSV (h^{-1})	$X_{propane}{}^{ab}$ (%)	$S_{propylene}{}^{ab}$ (%)	Ref.
Ga_2O_3/MCM-22	5	600	0.6	57.8(20.6)[c]	37.5(64.1)[c]	19
Ga_2O_3/ITQ-2	5	600	0.6	30.0(19.3)[c]	72.0(78.4)[c]	19
Ga_2O_3/HZSM-48	5	600	0.6	40.0(36.3)[c]	53.8(54.5)[c]	11
Ga_2O_3/ZSM-5	5	600	0.6	76.3(25.0)[c]	—	18
Ga_2O_3/TiO_2	5	600	0.6	23.0(3.0)[d]	85.0(—)[d]	16
Ga_2O_3/Al_2O_3	5	600	0.6	33.0(18.0)[d]	92.0(—)[d]	16
Ga_2O_3/ZrO_2	5	600	0.6	39.0(5.0)[d]	74.0(—)[d]	16
Ga_2O_3/SiO_2	5	600	0.6	7.2(6.5)[d]	92.0(—)[d]	16
Ga_2O_3/MgO	5	600	0.6	5.3(4.0)[d]	34.0(—)[d]	16
Ga_2O_3/Al_2O_3	5	620	0.6	46.0(15.6)[c]	95.2(93.1)[c]	This work
Ga_2O_3/ZSM-5	5	620	0.6	78.1(28.8)[c]	60.2(86.1)[c]	This work
Ga_2O_3/SiO_2	5	620	0.6	6.7(5.1)[c]	90.1(91.1)[c]	This work
Ga_2O_3/SBA-15	5	620	0.6	28.5(22.1)[c]	92.5(91.6)[c]	This work

[a] Note: the given data of $X_{propane}$ and $S_{propylene}$ are estimated according to the given curves in the literatures. [b] The values outside and inside the parenthesis are the data obtained in the initial and terminal times, respectively. [c] The propane conversion (%) and corresponding propylene selectivity (%) after reaction for 8 h. [d] The propane conversion (%) and corresponding propylene selectivity (%) after reaction for 3 h.

different samples in the range of 200–600 °C are markedly different, suggesting that the weight loss of these two samples are caused by the combustion of different coke species. Therefore, it can be concluded that the reaction time may play an important effect on the graphitization degree of coke.

Table 7 displays some reports about the catalytic performances of Ga_2O_3-based catalysts for propane dehydrogenation reaction. The initial and final propane conversions and propylene selectivities are collected. As can be seen from Table 7, the supports of catalyst have great influence on the catalytic performance, especially the propylene selectivity. The previous presented the low propylene selectivity and catalytic stability. However, the $5Ga_2O_3$/SBA-15 catalyst in this study displays the excellent catalytic stability accompanied with the relatively high conversion and selectivity, and the catalytic stability is evidently higher than those of the catalysts reported in literatures.

4 Conclusions

In this study, the influences of different supports (ZSM-5, SBA-15, γ-Al_2O_3 and SiO_2) and Ga_2O_3 loading on the properties and catalytic performances of supported Ga_2O_3 catalysts for propane dehydrogenation reaction were investigated. It can be found that the intrinsic nature of supports and the loading amount could strongly influence the textual properties, surface morphologies, acidic properties, dispersion of Ga species, surface chemical states and coke formation, bringing about the different catalytic performances of the corresponding catalysts. In particular, the strong acid sites of catalyst largely determine the dispersion of Ga species, but the strong acid sites also can induce adverse side reactions. Thus, for Ga_2O_3-supported catalysts in propane dehydrogenation reaction, striking an appropriate balance between the roles of strong acid sites in enhancing the reaction activity and that of decreasing the selectivity and stability is essential.

Among the catalysts with different supports, the $5Ga_2O_3$/ZSM-5 catalyst shows the best catalytic activity and the lowest catalytic stability, possesses the maximum gallium ions ($Ga^{\delta+}$ cations, $\delta < 2$), well-dispersed Ga species and strong acid sites. The $5Ga_2O_3$/SBA-15 catalyst exhibits the highest catalytic stability, the highest S_{BET} value and the lowest acidity. The propane conversion only declines 11% after reaction for 30 h. As for $x$$Ga_2O_3$/SBA-15 catalysts, the agglomeration degree of Ga species gradually increased as the increase of Ga_2O_3 loading amount. The $5Ga_2O_3$/SBA-15 sample exhibits the highest catalytic performance, possesses the most well-dispersed Ga species and the best structure accompany with the relatively high loading amount, the final propane conversion and propylene selectivity still attain above 17.5% and 92.0% after 30 h propane dehydrogenation reaction at 620 °C.

Acknowledgements

The research is supported by Science and Technology Commission of Shanghai Municipality (14520502900) and Internation Joint Laboratory on Resource Chemistry (IJLRC).

References

1 B. V. Vora, Development of Dehydrogenation Catalysts and Processes, *Top. Catal.*, 2012, **55**, 1297–1308.
2 F. Cavani, N. Ballarini and A. Cericola, Oxidative dehydrogenation of ethane and propane: How far from commercial implementation?, *Catal. Today*, 2007, **127**, 113–131.
3 A. Dinse, S. Khennache, B. Frank, C. Hess, R. Herbert, S. Wrabetz, R. Schloegl and R. Schomaecker, Oxidative dehydrogenation of propane on silica (SBA-15) supported vanadia catalysts: A kinetic investigation, *J. Mol. Catal. A: Chem.*, 2009, **307**, 43–50.
4 T. Ren, M. Patel and K. Blok, Olefins from conventional and heavy feedstocks: Energy use in steam cracking and alternative processes, *Energy*, 2006, **31**, 425–451.
5 F. T. Zangeneh, A. Taeb, K. Gholivand and S. Sahebdelfar, Thermodynamic equilibrium analysis of propane dehydrogenation with carbon dioxide and side reactions, *Chem. Eng. Commun.*, 2016, **203**, 557–565.
6 J. Beckers and G. Rothenberg, Sustainable selective oxidations using ceria-based materials, *Green Chem.*, 2010, **12**, 939.
7 G. Siddiqi, P. Sun, V. Galvita and A. T. Bell, Catalyst performance of novel Pt/Mg(Ga)(Al)O catalysts for alkane dehydrogenation, *J. Catal.*, 2010, **274**, 200–206.
8 G. Wang, H. Zhang, H. Wang, Q. Zhu, C. Li and H. Shan, The role of metallic Sn species in catalytic dehydrogenation of propane: Active component rather than only promoter, *J. Catal.*, 2016, **344**, 606–608.
9 T. A. Peters, O. Liron, R. Tschentscher, M. Sheintuch and R. Bredesen, Investigation of Pd-based membranes in propane dehydrogenation (PDH) processes, *Chem. Eng. J.*, 2016, **305**, 191–200.
10 L. Liu, Q.-F. Deng, B. Agula, T.-Z. Ren, Y.-P. Liu, B. Zhaorigetu and Z.-Y. Yuan, Synthesis of ordered mesoporous carbon materials and their catalytic performance in dehydrogenation of propane to propylene, *Catal. Today*, 2012, **186**, 35–41.
11 Y. Ren, J. Wang, W. Hua, Y. Yue and Z. Gao, Ga_2O_3/HZSM-48 for dehydrogenation of propane: Effect of acidity and pore geometry of support, *J. Ind. Eng. Chem.*, 2012, **18**, 731–736.
12 L. R. Mentasty, O. F. Gorriz and L. E. Cadus, Chromium oxide supported on different Al_2O_3 supports: catalytic propane dehydrogenation, *Ind. Eng. Chem. Res.*, 1999, **38**, 396–404.
13 J. G. Eon, R. Olier and J. C. Volta, Oxidative dehydrogenation of propane on γ-Al_2O_3 supported vanadium oxides, *J. Catal.*, 1994, **145**, 318–326.
14 K. Nakagawa, M. Okamura, N. Ikenaga, T. Suzuki and T. Kobayashi, Dehydrogenation of ethane over gallium oxide in the presence of carbon dioxide, *Chem. Commun.*, 1998, 1025–1026.
15 P. Michorczyk and J. Ogonowski, Dehydrogenation of propane to propene over gallium oxide in the presence of CO_2, *Appl. Catal., A*, 2003, **251**, 425–433.

16 B. Xu, B. Zheng, W. Hua, Y. Yue and Z. Gao, Support effect in dehydrogenation of propane in the presence of CO_2 over supported gallium oxide catalysts, *J. Catal.*, 2006, **239**, 470–477.

17 R. Koirala, R. Buechel, F. Krumeich, S. E. Pratsinis and A. Baiker, Oxidative dehydrogenation of ethane with CO_2 over flame-made Ga-loaded TiO_2, *ACS Catal.*, 2015, **5**, 690–702.

18 B. Xu, T. Li, B. Zheng, W. Hua, Y. Yue and Z. Gao, Enhanced stability of HZSM-5 supported Ga_2O_3 catalyst in propane dehydrogenation by dealumination, *Catal. Lett.*, 2007, **119**, 283–288.

19 J. Wang, F. Zhang, W. Hua, Y. Yue and Z. Gao, Dehydrogenation of propane over MWW-type zeolites supported gallium oxide, *Catal. Commun.*, 2012, **18**, 63–67.

20 Z. Shen, J. Liu, H. Xu, Y. Yue, W. Hua and W. Shen, Dehydrogenation of ethane to ethylene over a highly efficient Ga_2O_3/HZSM-5 catalyst in the presence of CO_2, *Appl. Catal., A*, 2009, **356**, 148–153.

21 B. Zheng, W. Hua, Y. Yue and Z. Gao, Dehydrogenation of propane to propene over different polymorphs of gallium oxide, *J. Catal.*, 2005, **232**, 143–151.

22 K. M. Dooley, C. Chang and G. L. Price, Effects of pretreatments on state of gallium and aromatization activity of gallium/ZSM-5 catalysts, *Appl. Catal., A*, 1992, **84**, 17–30.

23 G. D. Meitzner, E. Iglesia, J. E. Baumgartner and E. S. Huang, The chemical state of gallium in working alkane dehydrocyclodimerization datalysts. *In situ* Gallium *K*-Edge X-ray absorption spectroscopy, *J. Catal.*, 1993, **140**, 209–225.

24 J. A. Biscardi and E. Iglesia, Gallium-loaded zeolites and related systems structure and function of metal cations in light alkane reactions catalyzed by modified H-ZSM5, *Catal. Today*, 1996, **31**, 207–231.

25 A. Ausavasukhi and T. Sooknoi, Tunable activity of [Ga] HZSM-5 with H_2 treatment: Ethane dehydrogenation, *Catal. Commun.*, 2014, **45**, 63–68.

26 I. Nowak, Effect of H_2–O_2 pre-treatments on the state of gallium in Ga/H-ZSM-5 propane aromatisation catalysts, *Appl. Catal., A*, 2003, **251**, 107–120.

27 F. Klose, M. Joshi, C. Hamel and A. Seidel-Morgenstern, Selective oxidation of ethane over a VO_x/γ-Al_2O_3 catalyst-investigation of the reaction network, *Appl. Catal., A*, 2004, **260**, 101–110.

28 A. Qiao, V. N. Kalevaru, J. Radnik, A. Düvel, P. Heitjans, A. S. H. Kumar, P. S. S. Prasad, N. Lingaiah and A. Martin, Oxidative dehydrogenation of ethane to ethylene over V_2O_5/Al_2O_3 catalysts: effect of source of alumina on the catalytic performance, *Ind. Eng. Chem. Res.*, 2014, **53**, 18711–18721.

29 A. Qiu, E. Li and Y. Fan, Effect of support composition on catalytic performance of PtSn/ZSM-5 catalyst for propane dehydrogenation, *Chin. J. Catal.*, 2007, **28**, 970.

30 D. Liu, P. Bai, P. Wu, D. Han, Y. Chai and Z. Yan, Surface chemistry and catalytic performance of chromia/alumina catalysts derived from different potassium impregnation sequences, *Appl. Surf. Sci.*, 2015, **351**, 250–259.

31 F. Ying, J. Li, C. Huang, W. Weng and H. Wan, Direct synthesis and superior catalytic performance of V-containing SBA-15 mesoporous materials for oxidative dehydrogenation of propane, *Catal. Lett.*, 2007, **115**, 137–142.

32 Y. Duan, Y. Zhou, Y. Zhang, X. Sheng, S. Zhou and Z. Zhang, Effect of aluminum modification on catalytic properties of PtSn-based catalysts supported on SBA-15 for propane dehydrogenation, *J. Nat. Gas Chem.*, 2012, **21**, 207–214.

33 J. D. Sunseri, W. T. Cooper and J. G. Dorsey, Reducing residual silanol interactions in reversed-phase liquid chromatography: Thermal treatment of silica before derivatization, *J. Chromatogr. A*, 2003, **1011**, 23–29.

34 R. Srivastava, D. Srinivas and P. Ratnasamy, Sites for CO_2 activation over amine-functionalized mesoporous Ti (Al)-SBA-15 catalysts, *Microporous Mesoporous Mater.*, 2006, **90**, 314–326.

35 M. León, E. Diíaz, S. Bennici, A. Vega, S. Ordónez and A. Auroux, Adsorption of CO_2 on hydrotalcite-derived mixed oxides: sorption mechanisms and consequences for adsorption irreversibility, *Ind. Eng. Chem. Res.*, 2010, **49**, 3663–3671.

36 B. Solsona, T. Blasco, J. M. López Nieto, M. L. Peña, F. Rey and A. Vidal-Moya, Vanadium oxide supported on mesoporous MCM-41 as selective catalysts in the oxidative dehydrogenation of alkanes, *J. Catal.*, 2001, **203**, 443–452.

37 M. A. Smith, A. Zoelle, Y. Yang, R. M. Rioux, N. G. Hamilton, K. Amakawa, P. K. Nielsen and A. Trunschke, Surface roughness effects in the catalytic behavior of vanadia supported on SBA-15, *J. Catal.*, 2014, **312**, 170–178.

38 Y. Zhang, Y. Zhou, M. Tang, X. Liu and Y. Duan, Effect of La calcination temperature on catalytic performance of PtSnNaLa/ZSM-5 catalyst for propane dehydrogenation, *Chem. Eng. J.*, 2012, **181**, 530–537.

39 X. Liu, W.-Z. Lang, L.-L. Long, C.-L. Hu, L.-F. Chu and Y.-J. Guo, Improved catalytic performance in propane dehydrogenation of PtSn/γ-Al_2O_3 catalysts by doping indium, *Chem. Eng. J.*, 2014, **247**, 183–192.

40 C. H. Bartholomew, Mechanisms of catalyst deactivation, *Appl. Catal., A*, 2001, **212**, 17–60.

41 C. Yu, H. Xu, Q. Ge and W. Li, Properties of the metallic phase of zinc-doped platinum catalysts for propane dehydrogenation, *J. Mol. Catal. A: Chem.*, 2007, **266**, 80–87.

42 L. Brabec, M. Jeschke, R. Klik, J. Novakova, L. Kubelkova, D. Freude, V. Bosáček and J. Meusinger, Various types of Ga in MFI metallosilicates: characterization and catalytic activity, *Appl. Catal., A*, 1998, **167**, 309–320.

43 A. Ausavasukhi, T. Sooknoi and D. E. Resasco, Catalytic deoxygenation of benzaldehyde over gallium-modified ZSM-5 zeolite, *J. Catal.*, 2009, **268**, 68–78.

44 R. Carli, C. L. Bianchi, R. Giannantonio and V. Ragaini, Low temperature reduction of gallium in a Ga_2O_3/HZSM-5 catalyst, *J. Mol. Catal.*, 1993, **83**, 379–389.

45 S. E. Collins, M. A. Baltanás, J. L. G. Fierro and A. L. Bonivardi, Gallium–hydrogen bond formation on gallium and gallium–palladium silica-supported catalysts, *J. Catal.*, 2002, **211**, 252–264.

46 B. M. Reddy, I. Ganesh, E. P. Reddy, A. Fernández and P. G. Smirniotis, Surface characterization of Ga_2O_3-TiO_2 and V_2O_5/Ga_2O_3-TiO_2 catalysts, *J. Phys. Chem. B*, 2001, **105**, 6227–6235.

47 N. Rane, A. Overweg, V. Kazansky, R. Vansanten and E. Hensen, Characterization and reactivity of Ga^+ and GaO^+ cations in zeolite ZSM-5, *J. Catal.*, 2006, **239**, 478–485.

48 E. J. M. Hensen, M. García-Sánchez, N. Rane, P. C. M. M. Magusin, P.-H. Liu, K.-J. Chao and R. A. Van Santen, In situ Ga *K* edge XANES study of the activation of Ga/ZSM-5 prepared by chemical vapor deposition of trimethylgallium, *Catal. Lett.*, 2005, **101**, 79–85.

49 M. Guisnet and N. S. Gnep, Aromatization of propane over GaHMFI catalysts. Reaction scheme, nature of the dehydrogenating species and mode of coke formation, *Catal. Today*, 1996, **31**, 275–292.

50 P. Meriaudeau and M. Primet, FTIR study of hydrogen adsorption on α-Ga_2O_3, *J. Mol. Catal.*, 1990, **61**, 227–234.

51 B. K. Vu, M. B. Song, I. Y. Ahn, Y.-W. Suh, D. J. Suh, J. S. Kim and E. W. Shin, Location and structure of coke generated over Pt–Sn/Al_2O_3 in propane dehydrogenation, *J. Ind. Eng. Chem.*, 2011, **17**, 71–76.

52 Y. Zhang, Y. Zhou, L. Wan, M. Xue, Y. Duan and X. Liu, Effect of magnesium addition on catalytic performance of PtSnK/γ-Al_2O_3 catalyst for isobutane dehydrogenation, *Fuel Process. Technol.*, 2011, **92**, 1632–1638.

53 Y. Zhang, Y. Zhou, J. Shi, S. Zhou, Z. Zhang, S. Zhang and M. Guo, Propane dehydrogenation over PtSnNa/La-doped Al_2O_3 catalyst: effect of La content, *Fuel Process. Technol.*, 2013, **111**, 94–104.

54 Y. Zhang, Y. Zhou, L. Wan, M. Xue, Y. Duan and X. Liu, Synergistic effect between Sn and K promoters on supported platinum catalyst for isobutane dehydrogenation, *J. Nat. Gas Chem.*, 2011, **20**, 639–646.